

# Anomaly Detection in Hyperspectral Images of Complex Scenes

Dirk BORGHYS <sup>a,1</sup>, Elie TRUYEN <sup>a</sup> Michal SHIMONI <sup>a</sup> and Christiaan PERNEEL <sup>b</sup>

<sup>a</sup> *Royal Military Academy, Signal & Image Centre, Brussels, Belgium*

<sup>b</sup> *Royal Military Academy, Dept. of Applied Mathematics, Brussels, Belgium*

**Abstract.** The aim of anomaly detection in hyperspectral image processing is to detect pixels in the hyperspectral datacube that exhibit spectral signatures that are exceptional in the investigated scene. The current paper investigates the detection of anomalies in complex environments, i.e. urban and industrial scenes. The classical anomaly detection consists of a local measurement of differences between the spectral signature of the pixel and the average spectral signature of its surroundings. In complex environments such an approach is not adequate because of the high spatial variation of the background spectral features. Approaches based on global image segmentation have already been proposed in literature. This paper proposes a two-level segmentation based approach. In the first step of the method a scanning window is moved over the image. At each position a few characteristic spectra are determined. This is done either by spectral clustering or end-member selection methods. Then the image tile, defined by the current position of the scanning window, is classified using the determined spectra and only the spectra to which at least a given percentage of the image tile's pixels is assigned, are stored. At the end of the process the most characteristic spectra are searched within the collected set of spectra. This is again done by clustering or endmember selection. The final anomaly detection result is determined using a distance classifier or by spectral unmixing, based on the selected characteristic spectra. The method is tested and evaluated on three hyperspectral scenes with diverse complexity and acquired by three different airborne sensors. For evaluation purposes, the proposed methods are compared to two existing global image segmentation approaches and to the local Reed Xiaoli (RX) detector.

**Keywords.** Anomaly detection, segmentation, clustering, hyperspectral

## Introduction

Anomaly detection in hyperspectral data has received a lot of attention in the last years for various applications. The aim of anomaly detection is to detect pixels in the datacube whose spectra differ significantly from the background spectra. In anomaly detection no prior knowledge about the targets is assumed [1]. Anomaly detection methods in general estimate the spectra of the background (locally or globally) and then detect anomalies as pixels with a large spectral distance w.r.t. the determined background spectra. The Reed

---

<sup>1</sup>Corresponding Author: Dirk Borghys, Royal Military Academy, Signal & Image Centre, Renaissancelaan 30, B1000 Brussels, Belgium; E-mail: Dirk.Borghys@rma.ac.be.

Xiaoli (RX) algorithm [2], which is the benchmark anomaly detector for hyperspectral imagery, models the local background by a single multi-variate normal distribution. When the scene is highly structured, the single Gaussian assumption no longer adequate. A possible solution is to use Gaussian mixture models. The number of distributions, their weights, and the parameters of the normal distributions are then estimated by stochastic expectation maximization (SEM) method [3]. Sub-space detectors form another interesting family of anomaly detectors. In [4] several linear and non-linear (kernelized) sub-space detectors are compared and the Kernel Principle Component Analysis based detector (KPCA) [5] was found to give the best detection results for the scenes investigated in that paper. All of the above mentioned methods detect anomalies by considering the spectral difference between the current pixel and its immediate surroundings, i.e. they are based on local statistics. In highly structured scenes such as urban scenes, local detectors are likely to produce many (false) alarms due to the high variability of surface materials. An alternative approach for anomaly detection, more suited for such complex scenes, consists in applying a scene segmentation prior to the actual anomaly detection. Anomaly detection methods based on global scene segmentation have already been proposed [6]-[9]. In these segmentation-based anomaly detectors (SBAD) the result of scene segmentation is used to estimate typical background spectral signatures. Anomalies are then detected as pixels with a large spectral distance to the background spectral signatures.

A possible disadvantage of global SBAD methods is the fact that in a very heterogeneous scene some important background classes may be missed in global segmentation. The current paper therefore proposes anomaly detection based on two-level image segmentation. Two methods are proposed. The first one is based on clustering methods (two-level clustering method or TLCM) and the second on end-member selection (TLES). In these methods local segmentation results are combined to find characteristic spectra of the background in the scene. In the TLCM the final anomaly detection step is a distance classifier w.r.t. these spectra while the final TLES result is the residue of linear unmixing using the background end-members. This paper also proposes a simple anomaly detector based on the local spectral distance histogram.

The proposed anomaly detection methods are applied on several hyperspectral datascubes, acquired by different sensors over scenes with diverse complexity. The results are compared to two global SBAD methods as well as to the RX detector.

## 1. The dataset

The presented analysis was performed on a set of 3 hypercubes of scenes with various complexity, acquired by different airborne sensors. Table 1 presents the main characteristics of the dataset. The first column is the name by which the scenes will be referred further in this paper. The three sites show respectively a city, a rural village and an airfield with aerospace industry. Figure 1 shows parts of the three scenes. In the data analysis, for the Hymap data (OBP) the first and last channel were not used and for BJO the dataset was reduced in spatial resolution by a factor of 4 for computational reasons.

**Table 1.** Overview of the dataset

Name	Site	Sensor name	Nr of bands	Waveband	Spatial resolution
PAV	Pavia (It)	Rosis	102	430 nm - 834 nm	1.3 m
BJO	Bjoerkelangen (No)	HySpex	80	410 nm - 984 nm	0.20 m
OBP	Oberpfaffenhofen(Ge)	Hymap	126	444 nm - 2.45 $\mu\text{m}$	4 m

**Figure 1.** RGB color composite of parts of the different scenes. Left: PAV, centre: BJO, right: OBP

## 2. Anomaly detection methods

This paper proposes three new anomaly detectors. The first two are based on a two-level segmentation and the third one is based on local statistics. The proposed methods are described in 2.1 and 2.3.2. Their results are compared to different existing anomaly detection methods that can be categorized into two classes. The first class contains the global segmentation based methods, summarized in section 2.2 and the second class consists of methods based on local statistics. These are discussed in section 2.3. For each anomaly detector, its parameters are also given because they are referred to in the comparative evaluation.

### 2.1. Two level segmentation-based anomaly detection

Two of the anomaly detection methods proposed in this paper are based on the same philosophy: a scanning window runs over the image and at each position of the window the principle background spectra are determined using a segmentation method that is either based on clustering (TLCM: two-level clustering method) or end-member selection (TLES: two-level endmember selection). The principle background spectra are respectively the cluster centres or endmembers to which at least a minimum percentage  $MP$  of the pixels in the image tile are assigned by either clustering or linear unmixing. The stored spectra should thus represent the local image background. At the end of the process the most important spectra among the ones that were stored, are determined using the same method (i.e. using either clustering or endmember selection). These are used for the actual anomaly detection. Fig. 2 presents a general overview of approach. Specific details for TLCM and TLES are given below.

#### 2.1.1. Two-level clustering method (TLCM)

In this method local clustering results are combined to find the characteristic spectra of the scene's background. The used clustering technique is a k-means with a cosine

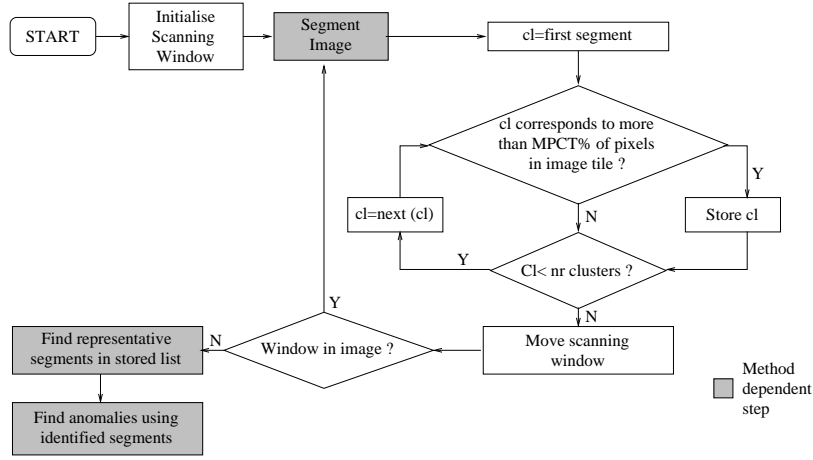


**Figure 2.** General flow diagram of the two-level segmentation methods

distance. The anomaly detector value in every pixel is the minimum of the spectral distances between its spectrum  $s$  and the background cluster centres  $cl(i)$ :  $A_{TLCM} = \min_i (distance(s, cl(i)))$

In this paper the spectral angle (TLCM-SA) and an extended binary encoding (TLCM-BE) [10] are used as spectral distances. The parameters of the method are:  $MP$  which is described above, the number of classes in the first clustering step  $N_1$  and the number of classes in the last clustering step  $N_2$ .

### 2.1.2. Two-level endmember selection based method (TLES)

In this method typical endmembers of the background are determined. Currently the endmember selection is based on the N-FINDR algorithm [11]. In the first phase of the TLES algorithm a fully-constrained linear spectral unmixing is applied, i.e. the spectra  $s$  in each pixel of the image tile is decomposed in terms of the  $N_{em}$  endmembers  $E_i$  as:

$$\min_{w_i} \left\| \sum_{i=1}^{N_{em}} E_i w_i - s \right\|^2 \quad \text{with } 0 \leq w_i \leq 1 \text{ and } \sum_i w_i = 1 \quad (1)$$

using a constrained least square approach.  $w_i$  is the abundance of endmember  $i$  in the linear mixture. The final anomaly detection result is the residue of the estimated mixture in each pixel:  $A_{TLES} = \| s - \sum_{i=1}^{N_{em}} E_i w_i \|$  For the linear unmixing in the final step, negative and superunity abundances are allowed [9], i.e. the condition  $0 \leq w_i \leq 1$  is not enforced in the last step. The parameters of the method are similar to those in TLCM:  $MP$  and the number of endmembers in the first and last application of the endmember selection  $N_1$  and  $N_2$ .

## 2.2. Global segmentation-based methods

### 2.2.1. The method of Blumberg (BLUM)

Two methods based on global image segmentation are included in the comparison. The first method (BLUM) was proposed by Blumberg [6]. A principal component analysis (PCA) is performed on the complete hypercube. The first 2 PCA bands are used to construct a 2-D histogram, which is segmented by locating its local maxima and attributing a given percentage of background pixels to each local maximum [6,12]. In the original paper by Blumberg the local maxima in the 2D histogram are determined using a scanning window. In the current paper a method based on mathematical morphology is used [13]. Parameters of the method are the number of bins ( $NBIN$ ) to construct the 2D histogram and the structuring element size ( $SES$ ) used for determining the local maxima.

### 2.2.2. Method based on self-organizing map (SOM)

The second method is based on a self-organizing map. A trained SOM is considered as a representation of the background classes in the scene. In [8] the resulting U-matrix is segmented based on its local minima's. In the current paper anomalies are determined by computing the spectral distances of the pixels from the SOM units as suggested in [9]. The SOM was applied on the first three PCA and run using a square map consisting of  $N_s \times N_s$  hexagonal cells. It was optimized sequentially and its only parameter is  $N_s$ . Contrary to [8] no spatial sub-sampling was applied here.

## 2.3. Local statistics-based methods

### 2.3.1. Local RX (LRX)

In LRX [2] the Mahalanobis distance is calculated between the current pixel and its local neighborhood defined by an outer window and separated from the current pixel by a guard window. In the implementation singular value decomposition is used for calculating the pseudo-inverse of the covariance matrix and the low values in the diagonal matrix are set to zero (cut-off is 99 % of the trace). Parameters of the method are guard window size ( $GWS$ ) and outer window size ( $OWS$ ).

### 2.3.2. Local histogram-based method (LHIS)

The third anomaly detector proposed in this paper is based on a local spectral distance histogram. The Euclidean distances are determined between the spectra of the current pixel and the pixels in its immediate neighborhood. The more the current pixel is different from its local background, the higher the mean of the histogram of these distances will be. This mean is used as the detection value. Like with RX, a dual window is used.

## 3. Experimental setup

Because the results of each detector depend on the choice of its parameters, the parameters were varied in a range that seemed reasonable and each time the parameter setting that yielded the best results were used in the comparison. The sets of parameter values used in the analysis for the different detectors are presented in table 2. For instance for BLUM  $3 \times 6$  settings of parameters were examined.

**Table 2.** Parameter sets used for the different detectors

Method	Parameter	Parameter Range	Method	Parameter	Parameter Range
TLCM-SA	MP	5,10,15	BLUM	SES	3,5,7
and	N1	3-9		NBIN	20,50,100,200,500,1000
TLCM-BE	N2	2,4,6,8,10,15,20	SOM	Ns	5, 10, 20, 40
TLES	MP	3,5	LRX	GWS	1x1,3x3,5x5,7x7
	N1	5,10,15,20	LHIS	OWS	7x7,9x9,11x11,13x13
	N2	2,4,6,8,10,15,20			

## 4. Results and evaluation

### 4.1. Definition of ground truth

For a quantitative evaluation it is necessary to have ground truth available about the anomalies in the scene. In complex environments such as urban or industrial scenes, it is far from obvious to define the ground truth a priori. What indeed are anomalies in such scenes? In this work we have postulated a definition of anomalies for each of the scenes. For the PAV scene the ground truth consists of all cars present in the image. For the BJO scene cars are also a prime target, but there seem to be several trampolines visible in the scene with a peculiar spectrum. These were also added to the ground truth. For OBP the aircraft on the airfield and trucks on the motorway were indicated as ground truth.

### 4.2. Comparative evaluation

For the quantitative evaluation, the detectors were applied using all combinations of the parameters presented in table 2. For each detection result a Receiver Operator Characteristic (ROC) curve was generated based on the ground truth. The area under the curve (AUC) was used as a comparison value. Because the aim is to compare the different detectors, for each detector the best AUC was determined over all parameter combinations. Tables 3-5 show these values for the three test datasets. The parameter values corresponding to these best results are also shown. The order of the parameters is the same as in table 2, i.e. for TLCM and TLES parameter set is defined as (MP,N1,N2), for LHIS and LRX:(GWS,OWS), for BLUM:(SES,NBIN) and for SOM:(Ns). In order to have an idea of the impact of the parameter choice on the results of each detector, the average and standard deviation of the AUC ( $\overline{AUC}$  and  $\sigma_{AUC}$ ) over the complete parameter set is also shown in the tables.

**Table 3.** Overview of the results for the PAV dataset

Method	Best AUC	Opt. param.	$\overline{AUC}$	$\sigma_{AUC}$	Method	Best AUC	Opt. param.	$\overline{AUC}$	$\sigma_{AUC}$
TLCM-SA	0.770	(15,4,10)	0.72	0.021	LRX	0.673	(1,4)	0.64	0.015
TLCM-BE	0.756	(15,3,10)	0.739	0.008	BLUM	0.723	(5,200)	0.65	0.03
TLES	<b>0.813</b>	(3,15,6)	0.70	0.077	SOM	0.777	(40)	0.76	0.023
LHIS	0.788	(3,7)	0.73	0.030					

**Table 4.** Overview of the results for the BJO dataset

Method	Best AUC	Opt. param.	$\overline{AUC}$	$\sigma_{AUC}$	Method	Best AUC	Opt. param.	$\overline{AUC}$	$\sigma_{AUC}$
TLCM-SA	0.738	(15,9,8)	0.61	0.045	LRX	0.786	(1,4)	0.79	0.010
TLCM-BE	0.755	(10,6,15)	0.68	0.053	BLUM	0.711	(3,20)	0.62	0.064
TLES	0.751	(5,15,10)	0.52	0.097	SOM	0.644	(5)	0.61	0.023
LHIS	<b>0.842</b>	(3,7)	0.82	0.012					

**Table 5.** Overview of the results for the OBP dataset

Method	Best AUC	Opt. param.	$\overline{AUC}$	$\sigma_{AUC}$	Method	Best AUC	Opt. param.	$\overline{AUC}$	$\sigma_{AUC}$
TLCM-SA	0.93	(10,6,20)	0.83	0.072	LRX	0.684	(1,9)	0.65	0.019
TLCM-BE	<b>0.97</b>	(15,3,15)	0.94	0.015	BLUM	0.88	(7,500)	0.78	0.081
TLES	<b>0.98</b>	(5,10,20)	0.74	0.21	SOM	0.86	(40)	0.83	0.018
LHIS	0.871	(3,7)	0.85	0.011					

The tables show that the best results for the different sites are obtained by different detectors. For the PAV site the TLES gives the best results, for BJO the LHIS detector gives the best results and for OBP the TLES and the two TLCM detectors give the best results. The RX detector, that is often presented as a benchmark for anomaly detection, does not perform that well in these scenes. This is probably due to the fact that the complexity of the scene makes the single Gaussian assumption less appropriate. It would be interesting to investigate class-conditional RX or a method based on Gaussian mixtures.

The global segmentation methods perform better than the local RX in two of the scenes (OBP and PAV). In BJO the LRX detector gives better results. The reason for this has to be investigated further.

As far as the influence of the results with the choice of parameters is concerned, the two local statistics based methods have the most consistent behaviour with respect to varying the parameters. The two-level segmentation methods' results are much more parameter dependent.

The optimal parameter set is most similar across the scenes for the LHIS detector.

For the PAV and BJO scene the best AUC values obtained are less than 0.85, which is not high. Because the AUC values were obtained as the optimal value obtained over a large set of parameters for most of the methods, this can not be due to a bad parameter setting. The low values are probably due to the fact that the ground truth comprises only part of the "true" spectral anomalies. The "false alarms" for each method should be investigated more closely in order to gain a better spectral and spatial understanding of the results. This topic will be addressed in further investigations.

## 5. Conclusions and further work

For the investigated datasets at least one of the anomaly detection methods proposed in this paper, gives better results than the two investigated methods based on global segmentation and the local RX detector. However, the best detector is different for each of the

scenes. The two-level segmentation methods give good results in two of the scenes, while the LHS detector gives the best results in one scene. This issue has to be investigated further.

For two of the scenes the best result obtained for the area under the ROC curve (AUC) is less than 0.85. We believe this is due to the fact that the ground truth comprises only part of the “true” spectral anomalies. In order to verify this a closer examination of the false alarms produced by the different methods will be carried out. In particular a spectroscopic and spatial analysis of results will be performed in order to gain a better understanding of the difference between the various detection methods.

In the next months we also intend to make a more thorough comparison of anomaly detector results in complex scenes including other anomaly detectors applied on more test datasets. In particular linear and non-linear sub-space detectors, gaussian-mixture based methods and methods based on support vector machines will be investigated.

### Acknowledgements

The PAV data were provided by Prof Gamba of the University of Pavia and acquired in the HySens campaign by DLR. Dr Skauli of the Norwegian Defense Research Institute (FFI) acquired and provided the BJO dataset. The OBP data acquisition was sponsored by the Belgian Science Policy and the flights were operated by the German DLR

### References

- [1] D.W.J. Stein, S.G Beaven, L.E. Hoff, E.M. Winter, A.P. Schaum, and A.D. Stocker, “Anomaly detection from hyperspectral imagery,” *IEEE Signal Proc. Mag.*, vol. 38, pp. 58–69, Jan 2002.
- [2] I.S. Reed and X. Yu, “Adaptive multiband cfar detection of an optical pattern with unknown spectral distribution,” *IEEE ASSP*, vol. 38, no. 10, pp. 1760–1770, Oct 1990.
- [3] C.J. Willis, “Anomaly detection in hyperspectral imagery using statistical mixture models,” in *Proc. 2nd EMRS DTC Technical Conference, 2005*.
- [4] H. Goldberg and N. Nasrabadi, “A comparative study of linear and nonlinear anomaly detectors for hyperspectral imagery,” in *Algorithms and Techn. for Multi-, Hyper-, and Ultraspectral Imagery XIII*. 2007, vol. 6565, SPIE.
- [5] B. Scholkopf, A.J. Smola, and K.R. Muller, “Kernel principal component analysis,” *Neural Computation*, vol. 10, pp. 1299–1319, 1999.
- [6] D.G. Blumberg, E. Ohel, and S.R. Rotman, “Anomaly detection in noisy multi and hyper spectral images of urban environments,” in *Proc. ISPRS 3rd URBAN Symp.*, Tempe, AZ, US, March 2005.
- [7] M.J. Carlotto, “A cluster-based approach for detecting man-made objects and changes in imagery,” *IEEE-TGRS*, vol. 43, no. 2, pp. 374–387, Feb 2005.
- [8] O. Duran and M. Petrou, “A time-efficient method for anomaly detection in hyperspectral images,” *IEEE-TGRS*, vol. 45, no. 12, pp. 3894–3904, Dec 2007.
- [9] O. Duran and M. Petrou, “Spectral unmixing with negative and superunity abundances for subpixel anomaly detection,” *IEEE-GRSL*, vol. 6, no. 1, pp. 152–156, Jan 2009.
- [10] A.S. Mazer, M. Martin, M. Lee, and J.E. Solomon, “Image processing software for imaging spectrometry data analysis,” *Remote Sensing of Environment*, vol. 24, pp. 201 – 210, 1988.
- [11] M.E. Winter, “Fast autonomous spectral endmember determination in hyperspectral data,” in *Proc. 13th Int. Conf. on Applied Geologic Remote Sensing*, Vancouver, CA, March 1999.
- [12] J. Silverman, S.R. Rotman, and C.E. Cafer, “Segmentation of multi-dimensional infrared imagery from histograms,” *Infrared Physics and Technology*, vol. 45, pp. 191–200, 2004.
- [13] D. Borghys, P. Verlinde, C. Perneel, and M. Acheroy, “Long range target detection in a cluttered environment using multi-sensor image sequences,” in *Proceedings on Signal Processing, Sensor Fusion and Target Recognition IV - SPIE - USA (Orlando)*, 20-25 April 1997.